DOI 10.4430/bgo00348

A novel approach based on the fast sigmoid function for interpretation of potential field data

E. Oksum[1], D.V. Le[2], M.D. Vu[3], T.-H.T. Nguyen[3] and L.T. Pham[3]

[1] *Department of Geophysical Engineering, Engineering Faculty, Süleyman Demirel University, Isparta, Turkey*

[2] *Institute of Geophysics, Vietnam Academy of Science and Technology, Hanoi, Vietnam*

[3] *Department of Geophysics, Faculty of Physics, University of Science, Vietnam National University, Hanoi, Vietnam*

(Received: 14 September 2020; accepted: 30 November 2020; published online: 20 September 2021)

ABSTRACT Edge detection of geological structures is an important objective in interpretation of potential field data. Although many methods have been proposed to highlight the edges of the subsurface structures, it is still the focus of many researchers to derive new techniques or enhance existing methods that can improve resolution within this scope. Here, we introduce an enhanced edge detection filter (*FSED*) based on a modified fast sigmoid function and the vertical and horizontal derivatives of the total horizontal gradient of the potential field data. The efficiency of the proposed filter was tested on synthetic data and the results were also compared with those obtained from other commonly used filters. The test results showed that the proposed filter could not only balance anomalies from shallow and deep sources, but also more accurately determine the edge location of these structures. The application of the proposed filter using real data was carried out on the gravity and magnetic data from Vietnam. For both the data, the *FSED* provided more detailed and clearer horizontal location of edges of causative structures. This filter is therefore promising to be a better tool for qualitative interpretation of potential field data compared to other popular filters.

Key words: algorithm, gravity, magnetics, image processing, interpretation.

1. Introduction

Interpretation of potential field data in terms of edge detection to delineate the horizontal boundaries of the subsurface structures is a frequently required task for geological mapping of a given region and for applications in environmental and engineering (Hsu *et al.*, 1996; Fedi and Florio, 2001; Zuo *et al.*, 2014; Eldosouky *et al.*, 2020c). Many edge detection filters have been developed to outline edges of the geological structures from potential field data, and most of these techniques are based on horizontal and vertical derivatives of the field or their various combinations (Kafadar, 2017; Pham *et al.*, 2018b; Oksum *et al.*, 2019; Eldosouky *et al.*, 2020a). Cordell and Grauch (1985) proposed the use of the peak values of the total horizontal gradient (*THG*) of the field *F* to recognise the edge location of source bodies. The filter is given by:

$$THG = \sqrt{\left(\frac{\partial F}{\partial x}\right)^2 + \left(\frac{\partial F}{\partial y}\right)^2}. \quad (1)$$

Roest *et al.* (1992) proposed the total gradient (*TG*) that uses maximum values to detect geological structures. The filter is expressed as:

$$TG = \sqrt{\left(\frac{\partial F}{\partial x}\right)^2 + \left(\frac{\partial F}{\partial y}\right)^2 + \left(\frac{\partial F}{\partial z}\right)^2}. \quad (2)$$

The drawback of the *THG* and *TG* methods is that they cannot balance anomalies with low and high amplitudes simultaneously (Pham *et al.*, 2018a, 2019; Eldosouky, 2019; Eldosouky and Saada, 2020; Pham, 2020).

In recent years, there has been a rapid development of methods for the ability to balance the anomalies with different amplitudes. Miller and Singh (1994) introduced the first balanced edge detection filter, called the tilt angle (*TA*), which is the arctangent of the ratio of the vertical derivative to total horizontal derivative of the field:

$$TA = atan \frac{\frac{\partial F}{\partial z}}{\sqrt{\left(\frac{\partial F}{\partial x}\right)^2 + \left(\frac{\partial F}{\partial y}\right)^2}}. \quad (3)$$

Verduzco *et al.* (2004) suggested the use of the total horizontal gradient of the tilt angle (*THG_TA*) for better resolution in delineating the edges. The filter is given by:

$$THG\_TA = \sqrt{\left(\frac{\partial TA}{\partial x}\right)^2 + \left(\frac{\partial TA}{\partial y}\right)^2}. \quad (4)$$

Wijns *et al.* (2005) proposed another balanced edge detector filter, called the theta map (*TM*), where the *THG* is normalised by the total gradient:

$$TM = acos \frac{\sqrt{\left(\frac{\partial F}{\partial x}\right)^2 + \left(\frac{\partial F}{\partial y}\right)^2}}{TG}. \quad (5)$$

Ferreira *et al.* (2013) introduced the tilt angle of the total horizontal gradient (*TTHG*) as a modified version of the *TA*. They showed that the method is more effective in improving the edges of deep geological bodies compared with the other methods. The filter is given by:

$$TTHG = atan \frac{\frac{\partial THG}{\partial z}}{\sqrt{\left(\frac{\partial THG}{\partial x}\right)^2 + \left(\frac{\partial THG}{\partial y}\right)^2}}. \quad (6)$$

Another method by Cooper (2014) used the tilt angle of the analytical signal amplitude (*TTG*) as an edge detector filter, which is expressed as:

$$TTG = atan \frac{\frac{\partial TG}{\partial z}}{\sqrt{\left(\frac{\partial TG}{\partial x}\right)^2 + \left(\frac{\partial TG}{\partial y}\right)^2}}. \quad (7)$$

The concept of edge enhancement is not limited only to the above given methods. Several authors have introduced different methods to detect the edges of geological sources (e.g. Hsu *et al.*, 1996; Sertcelik and Kafadar, 2012; Oruç *et al.*, 2013; Ma *et al.*, 2014; Yuan and Yu, 2014; Foks and Li, 2016; Nasuti and Nasuti, 2018; among others).

In this paper, we propose an improved edge detector filter that uses a modified fast sigmoid function to enhance the total horizontal gradient of potential field anomalies. The effectiveness of the proposed method is demonstrated on synthetic gravity data produced by model structures with different sizes and depths, as well as on real magnetic and gravity data from the Tuan Giao area, north-western Vietnam.

2. Method

We proposed an approach to increase the resolution and accuracy of the estimated edges from an enhancement of the total horizontal gradient of the potential field anomalies. The proposed method utilises a modified fast sigmoid function of the ratio of the first-order vertical and horizontal derivatives of the total horizontal gradient of the potential field, defined as:

$$FSED = \frac{R-1}{1+|R|}. \quad (8)$$

where:

$$R = \frac{\frac{\partial THG}{\partial z}}{\sqrt{\left(\frac{\partial THG}{\partial x}\right)^2 + \left(\frac{\partial THG}{\partial y}\right)^2}}. \quad (9)$$

FSED is fast in the calculation and easy to implement. The *FSED* filter provides maximum amplitudes on the edges of the anomalous sources. Since the filter design is based on the ratio of the derivatives of the total horizontal gradient, it can simultaneously balance anomalies from deep and shallow geological sources.

In the next section, we compare the *FSED* with some commonly used edge detection filters to show the effectiveness of the proposed filter. These filters are *THG* (Cordell and Grauch, 1985), *TG* (Roest *et al.*, 1992), *TA* (Miller and Singh, 1994), *THG_TA* (Verduzco *et al.*, 2004), *TM* (Wijns *et al.,* 2005), *TTHG* (Ferreira *et al.*, 2013), and *TTG* (Cooper, 2014).

3. Application to synthetic data

The first synthetic model is composed of three magnetised prismatic bodies. Figs. 1a and 1b show the three-dimensional and plan views of the first synthetic model, respectively. The parameters of each prism are listed in Table 1. Here, the prisms are the same in size but located

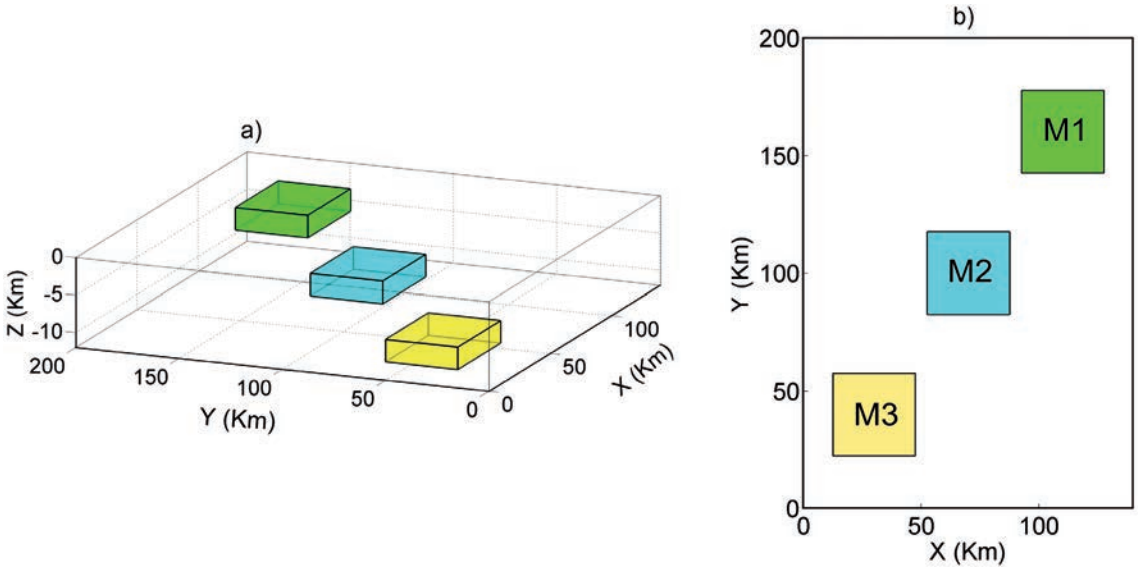

Fig. 1 - Three-dimensional view (a) and plan view (b) of the first synthetic model.

Table 1 - The parameters of the first synthetic model shown in Fig. 1.

Parameters / Prism ID	M1	M2	M3
Centre coordinates (km; km)	110; 160	70; 100	30; 40
Width (direction *x*) (km)	35	35	35
Length (direction *y*) (km)	35	35	35
Depth of top (km)	2	5	8
Depth of bottom (km)	5	8	11
Declination (°)	0	0	0
Inclination (°)	90	90	90
Magnetization (A/m)	2	-2	2

at different depths. The magnetic anomalies due to the prisms were calculated on a regular grid of 201×141 observation points with a spacing of 1 km. The theoretical magnetic data shown in Fig. 2a. Figs. 2b and 2c indicate the obtained results from application of the *THG* and *TG* methods, respectively. The maximum values of the *THG* and *TG* display the edges of the anomalous sources. As it can be seen from Figs. 2b and 2c, although the *THG* and *TG* methods can highlight the edges of the relatively shallow causative body (labelled as M1 in Fig. 1b), they do not give a clear result for the deeper bodies (labelled as M2 and M3 in Fig. 1b). Figs. 2d and 2e show the *TA* and its total horizontal gradient (*THG_TA*), respectively. The *TA* values are maximal

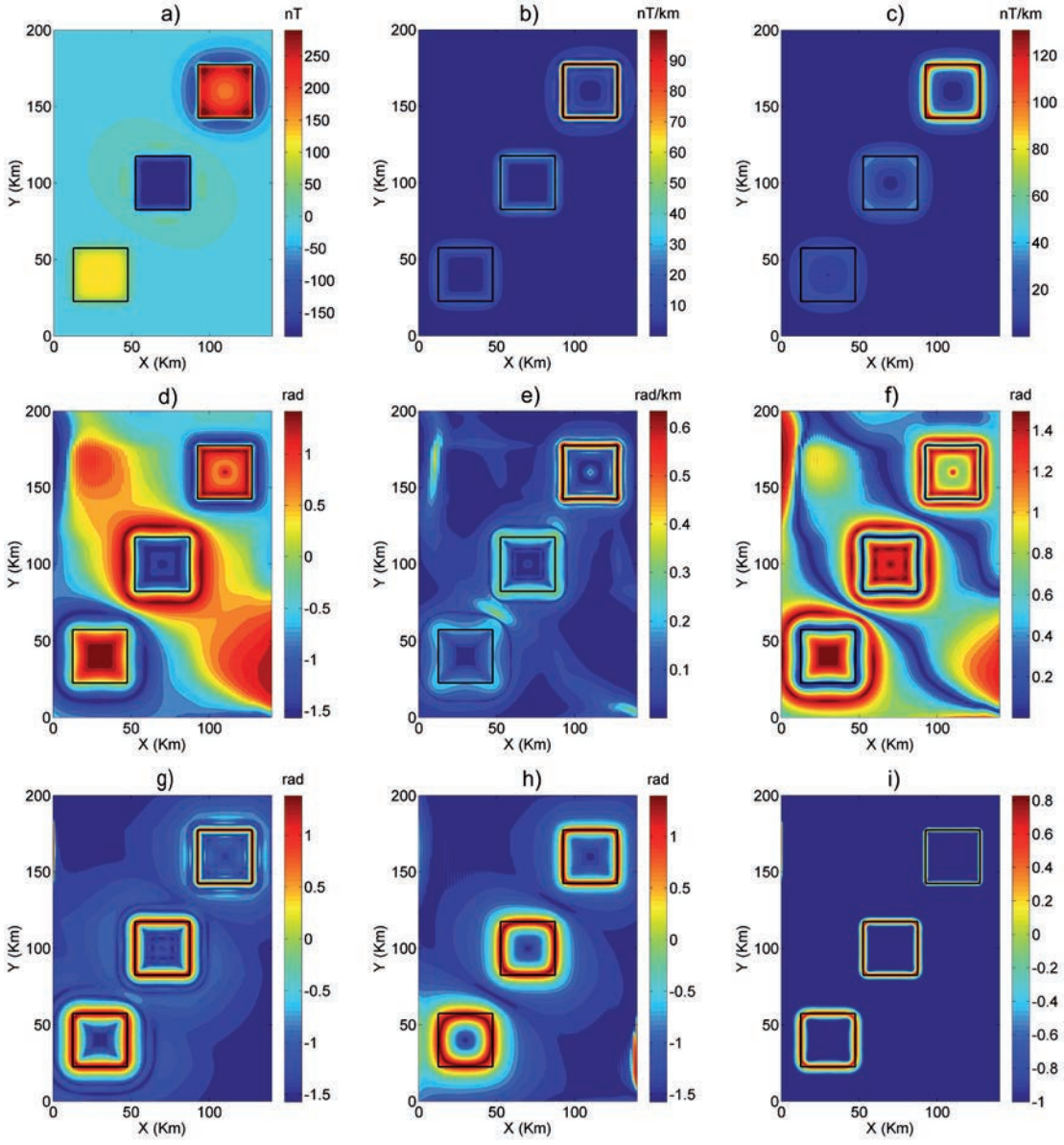

Fig. 2 - For synthetic model in Fig. 1: a) synthetic magnetic anomaly due to the three-prism model of positive density contrasts, b) *THG*, c) *TG*, d) *TA*, e) *THG_TA*, f) *TM*, g) *TTHG*, h) *TTG*, i) *FSED*.

or minimal over the centre of each prismatic body. Thus, it may be stated that the filter is not primarily an edge detector, as pointed out by Eldosouky *et al.* (2020b) and Pham *et al.* (2020). The *THG_TA* is able to delineate the edges of the shallowest body. However, it still does not give a clear result for the deep sources (labelled as M2 and M3 in Fig. 1b). Fig. 2f shows the *TM* map. The *TM* method produces minimum values over the edges of each prism. Although the method can distinguish the bodies significantly better than *THG*, *TG*, and *THG_TA*, it brings the secondary edges between the bodies. Figs. 2g and 2h show the *TTHG* and *TTG* maps, respectively. The located maxima of the *TTHG* show a better estimation of the source edges than the *TM*. The *TTG* can balance the anomaly amplitudes generated by the sources located at different depths, but

for the deepest source (labelled as M3 in Fig. 1b), the peaks of the *TTG* appear inwards from the edges, making the body seem smaller than it is. The *FSED* of the gravity data in Fig. 2a is shown in Fig. 2i. It can be clearly seen that the *FSED* filter can improve the source edges more clearly and precisely than other filters. The *FSED* also provides an image of the source edges with higher resolution, compared with the *TTHG* and other filters.

The second synthetic model is composed of three thin bodies (G1, G2, and G3) and two overlapped bodies (G4 and G5). This model contains both the positive and negative density contrast structures. Figs. 3a and 3b show the three-dimensional and plan views of the second synthetic model, respectively. The parameters of each prism are listed in Table 2. The gravity anomalies due to the prisms were calculated on a regular grid of 201×141 observation points with a spacing of

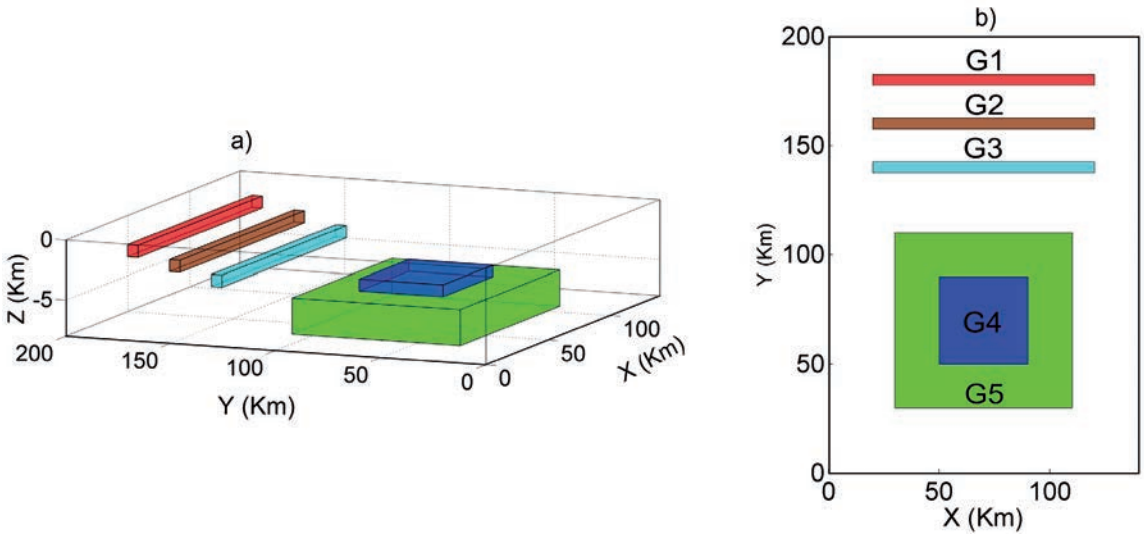

Fig. 3 - Three-dimensional view (a) and plan view (b) of the second synthetic model.

1 km. Fig. 4a demonstrates the gravity anomaly map of the second synthetic model. The *THG* of the gravity data is shown in Fig. 4b. The *THG* can well recognise the edges of the sources G1 and G5, but cannot clearly define the edges of the sources G2, G3 and G4. Fig 4c shows the *TG* of the data. In this case, the method cannot extract the boundaries of the thin sources G1, G2, G3, and it does not give a clear result for the source G4. Figs. 4d to 4f show the *TA*, *THG_TA*, and *TM*, respectively.

Table 2 - The parameters of the second synthetic model shown in Fig. 3.

Parameters / Prism ID	G1	G2	G3	G4	G5
Centre coordinates (km; km)	70; 180	70; 160	70; 140	70; 70	70; 70
Width (direction *x*) (km)	5	5	5	40	80
Length (direction *y*) (km)	100	100	100	40	80
Depth of top (km)	1	2	3	4	5
Depth of bottom (km)	2	3	4	5	8
Density contrast (g/cm^3)	0.3	-0.3	0.3	-0.2	0.3

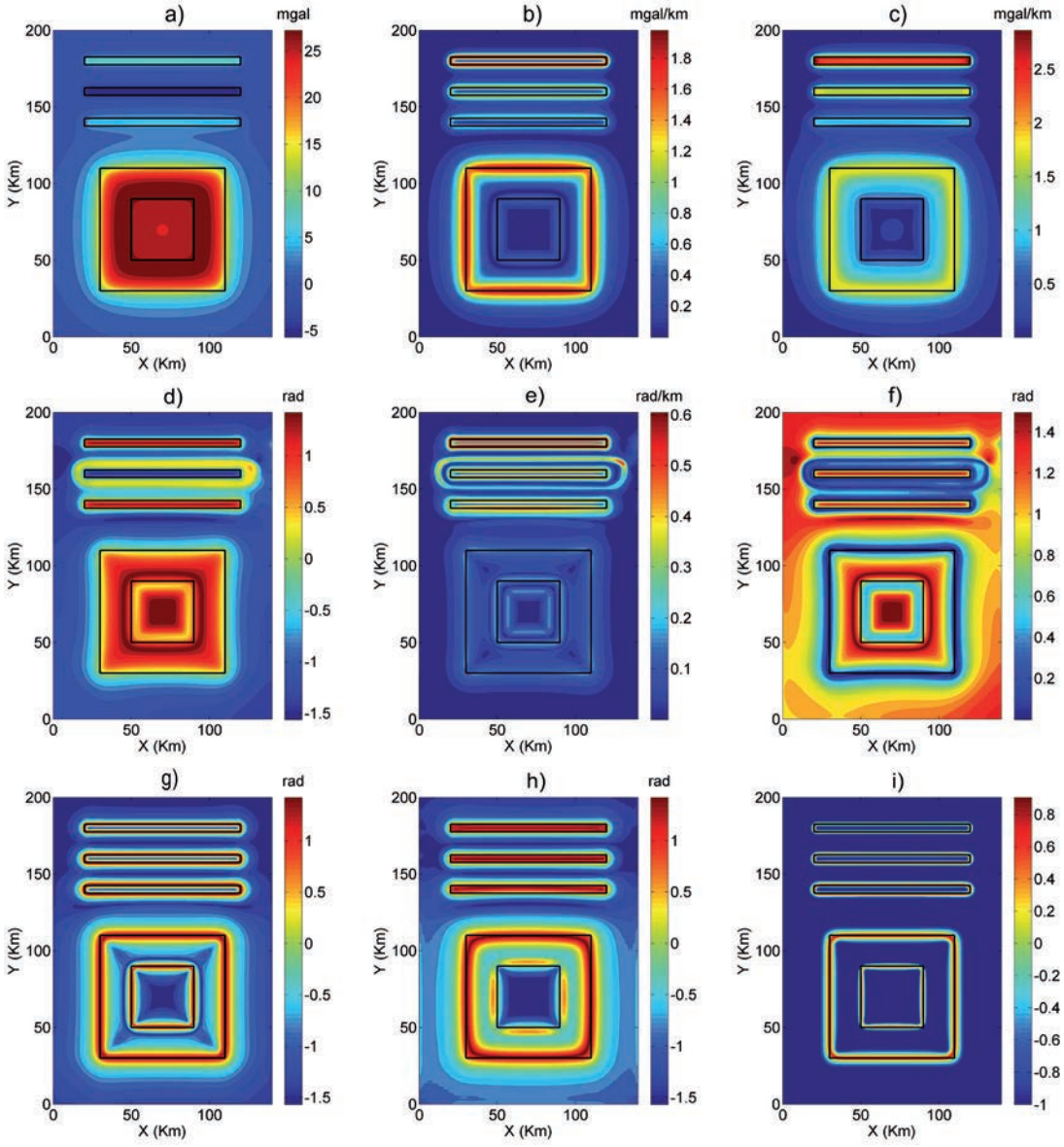

Fig. 4 - For synthetic model in Fig. 3: a) synthetic gravity anomaly due to the five-prism model, b) *THG*, c) *TG*, d) *TA*, e) *THG_TA*, f) *TM*, g) *TTHG*, h) *TTG*, i) *FSED*.

Although the *TA* is able to equalise the anomaly amplitudes of the source bodies with different depths, it produces false edges around the source G2. The edges of the shallowest source G1 by the *THG_TA* are clearly enhanced, but nevertheless, the edges of the deep-seated source are not well defined. Even worse, the filter produces spurious maxima over the body G4 and around the source G2. We can see from Fig. 4f that the *TM* brings false edge information when the model includes both positive and negative density bodies. For the source G4, the minima of the *TM* are shifted inwards from the edges, making the body seem smaller than it is. Figs. 4g and 4h demonstrate the image maps obtained from the application of the *TTHG* and *TTG* filters, respectively. We can see that the *TTHG* can well locate the source edges, although the edges of the deepest body are not

sharply defined. The *TTG* filter is able to detect the edges of the source G5, but it cannot outline the edges of the thin body and the recognised edges of the source G4 represent the structure larger than its true size. Fig. 4i depicts the *FSED* of the data in Fig. 4a. It can be seen that the sharpness of the edges obtained from the *FSED* filter is better than the *TTHG* filter. The *FSED* also can avoid generating additional false edges when the model contains both positive and negative contrast densities. Compared to the other filters, the proposed filter provides a much better performance in enhancing the edges of causative bodies.

In order to evaluate the performance of the proposed filter in noisy environment, we consider the third example. Here, the synthetic gravity data in Fig. 4a was contaminated with additive random noise with amplitude of 2% of the anomaly amplitude. Fig. 5a shows the noisecorrupted gravity anomaly map. To reduce the noise effect, an upward continuation of 1.5 km is applied to the noise-corrupted data prior to the edge detections. Figs. 5b to 5f illustrate the *THG*, *TG*, *TA*, *THG_TA*, and *TM* after the upward continuation of the data in Fig. 5a. Clearly, the *THG* and *TG* are not a balanced function, and the edges obtained from these methods are divergent. Furthermore, the *TG* map does not show the edges of the thin sources G1, G2, and G3, and the source G4 (Fig. 5c). We can see from Fig. 5e that, in this case, the *THG_TA* cannot extract the boundaries of the sources G4 and G5, and it brings the secondary edges around the source G2. The results obtained from using the *TA* and *TM* filters show that, although these filters are more effective in balancing high and low amplitude anomalies, they still bring some additional false edges. Figs. 5g to 5i display the *TTHG*, *TTG*, and *FSED* of the gravity data after applying an upward continuation of 1.5 km. It is clear that the *TTG* is more sensitive to noise than the *TTHG* and *FSED*. The method is also ineffective in revealing the edges of thin sources. The *TTHG* and *FSED* filters can effectively balance the amplitudes of the anomalies generated by the causative bodies located at different depths, and there are no false edges in their maps. By comparing the edge detection results of these filters, we can see that the *TTHG* and *FSED* filters provide better delineation of the edges of anomalous bodies compared to *THG*, *TG*, *TA*, *THG_TA*, *TM*, and *TTG* filters. However, the *FSED* filter produces an image with higher resolution, which is easier to interpret.

4. Real field data applications

To illustrate the effectiveness of the proposed filter in a real case, we apply the *FSED* to real gravity and magnetic data from the Tuan Giao area and compare the edge detection results with those of other filters. The study area is situated in north-western Vietnam and extends between latitudes 20.97° and 22.38° N, and longitudes 102.98° and 104.03° E (Fig. 6a). The area belongs to the South China and Indochina blocks, and is a region of high seismicity (Findlay and Phan, 1997; Nguyen *et al.*, 2018). The boundary between these blocks is located along the Song Ma suture zone (Lin *et al.*, 2009; Liu *et al.*, 2012). The recent geodynamics of the Tuan Giao area is conditioned by the collision between the Indo-Australian and Eurasian plates, and the subduction of the Pacific plate under the Eurasian plate (Nguyen *et al.*, 2018). Fig. 6b shows the geological map of the area (modified from Zhou *et al.*, 2013). The structural geology of the area is complicated with many major NW-SE trending faults that represent the main dividing boundaries of zones and tectonic regions. These faults are likely to generate the greatest earthquakes recorded in Vietnam, including the 1935 Dien Bien earthquake with M = 6.7 and the 1983 Tuan Giao earthquake with M = 6.8 (Bui and Nguyen, 2017). Following Khuong (2010), most lithologies of the Tuan Giao area are Mesozoic sedimentary sequences that include acidic volcanic, terrigenous sedimentary and carbonates rocks. Neoproterozoic, Proterozoic, Cenozoic and Paleozoic rocks consist of flysch, phyllites, carbonates sedimentary rocks, basalts, and schists, and Quaternary sediments also occur in the area.

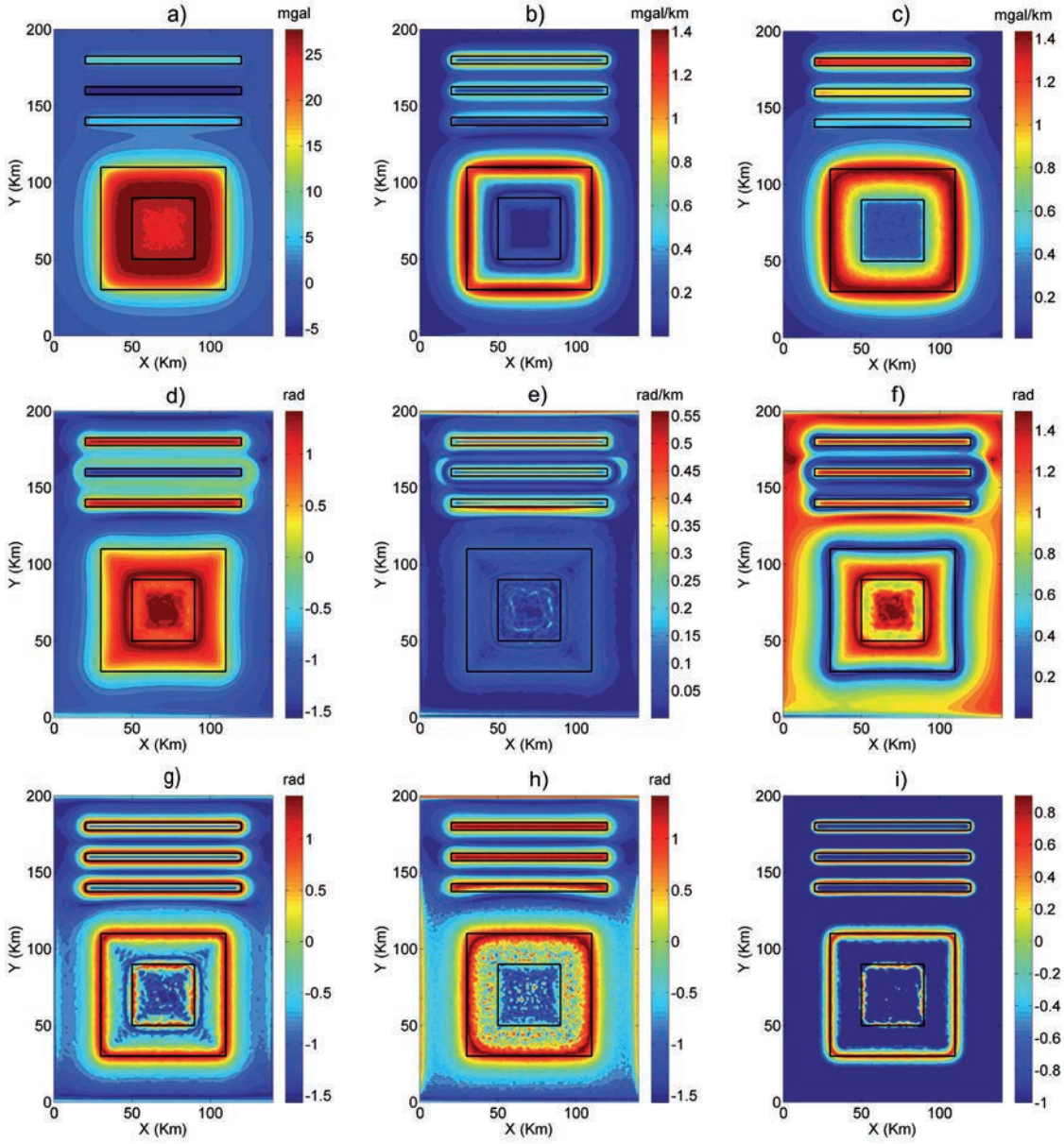

Fig. 5 - For synthetic model in Fig. 3: a) noise-corrupted synthetic gravity anomaly due to the five-prism model, b) *THG*, c) *TG*, d) *TA*, e) *THG_TA*, f) *TM*, g) *TTHG*, h) *TTG*, i) *FSED*.

Fig. 7a shows the reduction to the pole map of the aeromagnetic data in the Tuan Giao area (Minh *et al.*, 2001). In order to reduce the noise effects in the data, we also applied an upward continuation filter to an elevation of 0.5 km prior to the application of edge detector filters. Figs. 7b to 7i show the results obtained from using *THG*, *TG*, *TA*, *THG_TA*, *TM*, *TTHG*, *TTG*, and *FSED*, respectively. Clearly, high-amplitude anomalies dominate the *THG* and *TG* filters, and the edges of the low-amplitude anomalies are very blurred. Although the *TA* is more effective in balancing the different amplitude anomalies, it cannot clearly delineate the boundaries of geological units. As described above, the *THG_TA* and *TM* may bring to false geological boundaries. Moreover,

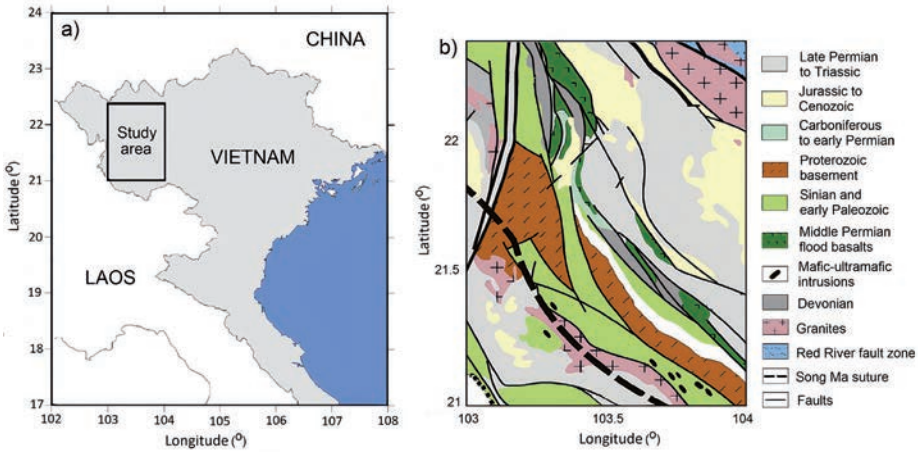

Fig. 6 - Location of the Tuan Giao region (a) and the simplified geological map (b) of the study area (Zhou *et al.*, 2013).

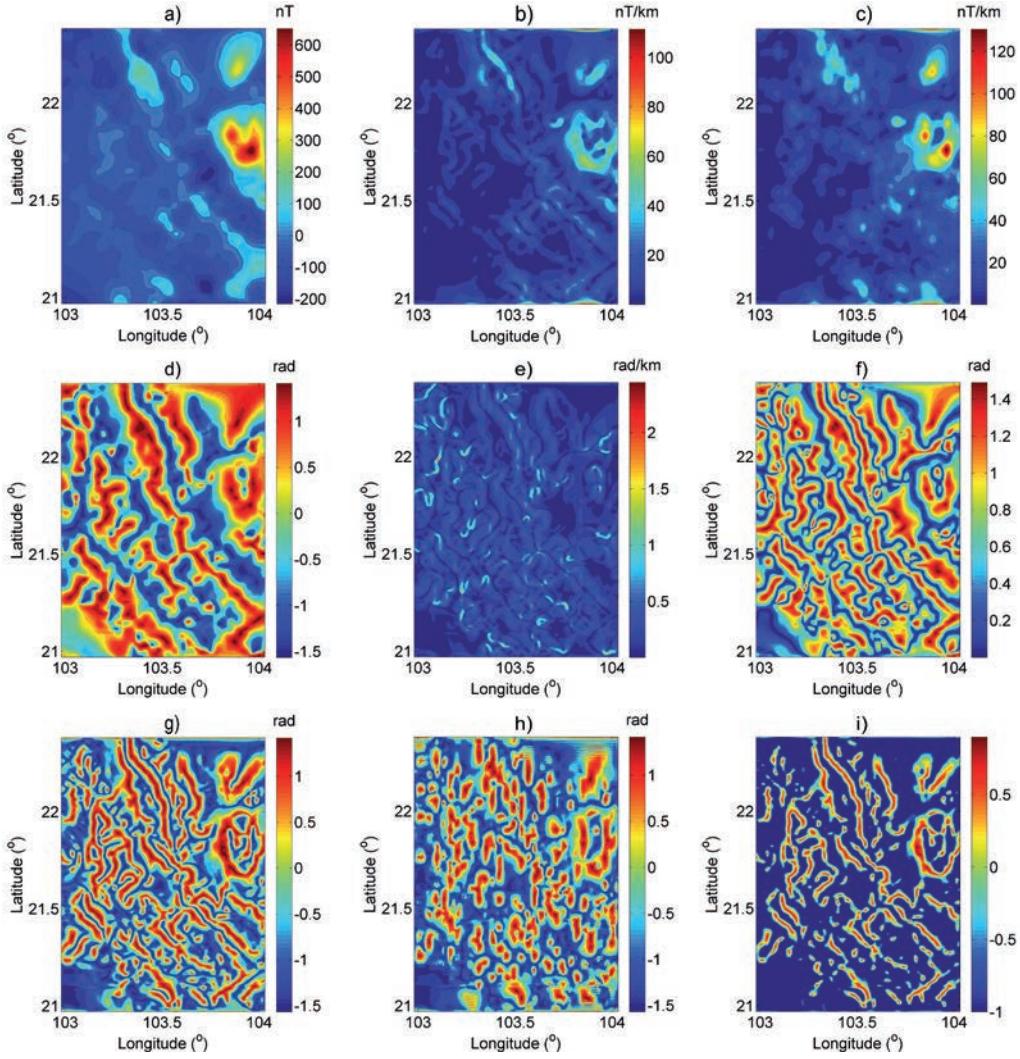

Fig. 7 - Real field application of the edge detection filters to the aeromagnetic data of Tuan Giao area, Vietnam: a) aeromagnetic map (*RTP*) of the study area, b) *THG*, c) *TG*, d) *TA*, e) *THG_TA*, f) *TM*, g) *TTHG*, h) *TTG*, i) *FSED*.

many adjacent boundaries in the *THG_TA* and *TM* maps are connected, complicating the interpretation of geological features. Because the *TTG* filter uses the vertical derivative of the analytic signal amplitude, it is more sensitive to noise, compared with the other methods. As it can be seen from Figs. 6h and 6i, the anomalies determined by the *TTHG* and *FSED* filters are more effective in enhancing the main magnetic structures. The *TTHG* and *FSED* maps show NW-SE trending magnetic structures, with many maximum values indicating the boundaries of basaltic formations. However, the results obtained from applying the *FSED* provide sharper edges. By and large, there is a good correlation between the horizontal locations of the magnetic structures obtained from the proposed filter and NW-SE trending geological features.

Fig. 8a shows the Bouguer gravity anomaly map of the Tuan Giao area (Pham *et al.*, 2020). The presence of a strong NW-SE trend in the gravity map is remarkable. Prior to the use of edge detection filters, an upward continuation of 2 km is applied to the gravity data in order

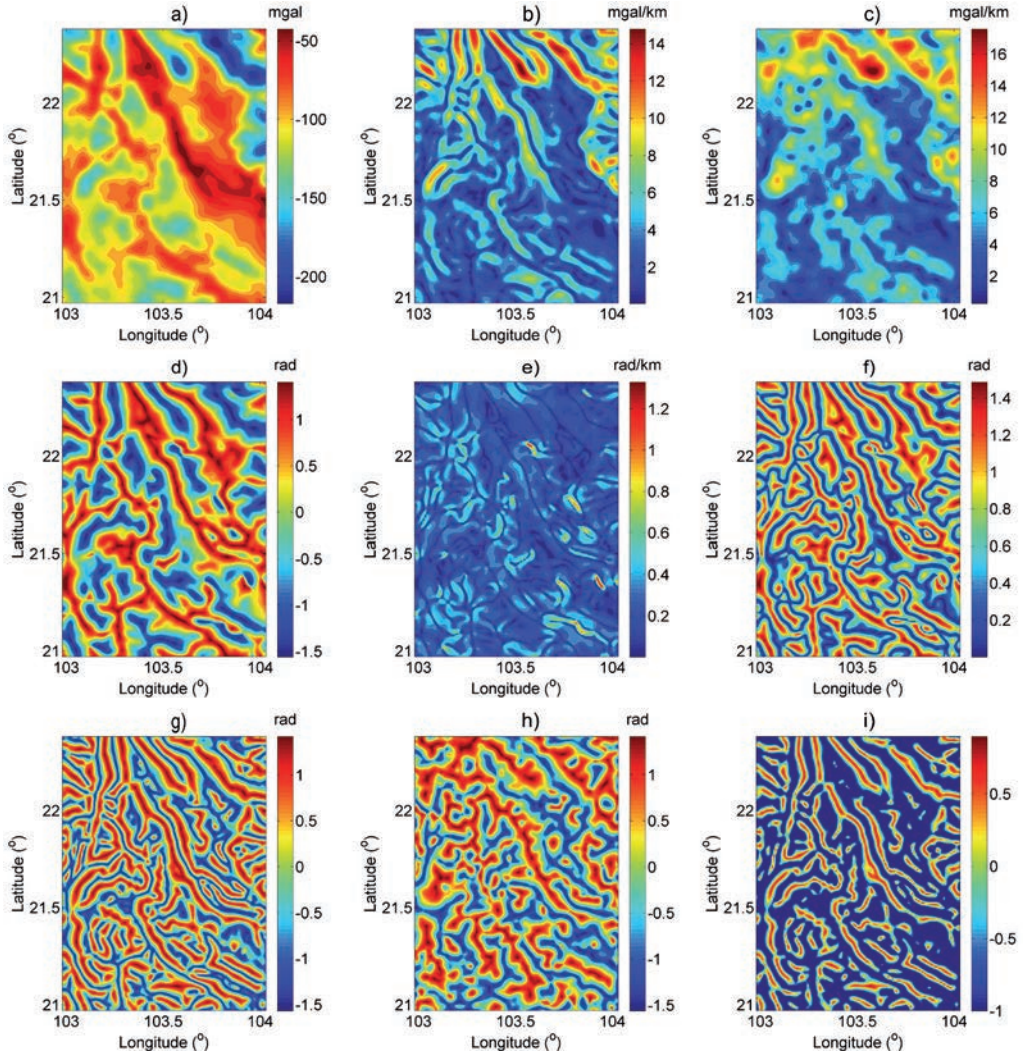

Fig. 8 - Real field application of the edge detection filters to the gravity anomaly data of the Tuan Giao area, Vietnam: a) Bouguer gravity map of the study area, b) *THG*, c) *TG*, d) *TA*, e) *THG_TA*, f) *TM*, g) *TTHG*, h) *TTG*, i) *FSED*.

to reduce the noise effects, and also to improve the effects of deep structures. Figs. 8b to 8i show the *THG*, *TG*, *TA*, *THG_TA*, *TM*, *TTHG*, *TTG*, and *FSED* of the transformed gravity data, respectively. The results generated by the *THG*, *TG*, *TA*, and *THG_TA* filters once again show that they do not present well the source edges. Since the *TTG* is sensitive to noise and the real gravity data are tainted with some noise, the results obtained from the *TTG* is less effective in delineating the edges of the source. In this case, the obtained image maps from the application of the *TM*, *TTHG*, and *FSED* filters allow us to highlight the source edges, and display the edges of the large and small amplitude anomalies clearly. These maps also provide evidence for determining the faults of the area. By comparing the results obtained by the *FSED* filter with those obtained by other filters, we can see that, although the *TM*, *TTHG*, and *FSED* filters can balance the amplitudes of the large and small anomalies, the *FSED* map significantly shows an improved resolution with more clearly source boundaries. As shown in Fig. 8i, the *FSED* map patterns a dominant NW-SE structural trend of sources that compares favourably with the complex geological structures of the area. On the other hand, the peaks of the *FSED* show a good correlation with many NW-SE trending faults in the study area.

5. Conclusions

We presented a new approach for edge enhancement of potential field data based on a modified fast sigmoid function and the total horizontal gradient. The effectiveness of this filter was tested using both synthetic gravity data and real potential field data sets from Vietnam. The outcomes from the application of the filter were also compared with those of other existing popular methods. Synthetic applications designed for various scenarios have shown that the proposed filter can balance the large and small amplitude anomalies due to sources of different depths and properties, as well as the edges of the sources are determined with higher resolution and more accurately. As another advantage, this filter also does not produce false edges when the anomalous sources contain opposite sign density contrasts simultaneously. The obtained results from the application of the filter to the gravity and aeromagnetic data of Vietnam are in agreement with the main geological structures of the area. In both the real field data applications, the proposed filter provided the best resolution and delineated the edges more clearly compared with the other utilised edge detection methods. The results revealed that the proposed edge detector filter *FSED* can be an effective tool in interpreting of potential field data to determine edges of both shallow and deep structures.

Acknowledgements. This research is funded by the Vietnam National University, Hanoi (VNU) under project number QG.20.13.

REFERENCES

Bui D.V. and Nguyen D.A.; 2017: *The relation between fault movement potential and seismic activity of major faults in north-western Vietnam*. Vietnam J. Earth Sci., 39, 240-255.

Cooper G.R.J.; 2014: *Reducing the dependence of the analytic signal amplitude of aeromagnetic data on the source vector direction*. Geophys., 79, J55-J60.

Cordell L. and Grauch V.J.S.; 1985: *Mapping basement magnetization zones from aeromagnetic data in the San Juan Basin, New Mexico*. In: Hinze W.J. (ed), The utility of regional gravity and magnetic anomaly maps, Society of Exploration Geophysics, Tulsa, OK, USA, pp. 181-197, doi: 10.1190/1.0931830346.ch16.

Eldosouky A.M.; 2019: *Aeromagnetic data for mapping geologic contacts at Samr El-Qaa area, north Eastern Desert, Egypt*. Arabian J. Geosci., 12, 2, doi: 10.1007/s12517-018-4182-2.

Eldosouky A.M. and Saada S.A; 2020: *Source edge detection (SED) of aeromagnetic data: synthetic examples and a case study from Haimur area, south Eastern Desert, Egypt*. Arabian J. Geosci., 13, 1-12.

Eldosouky A.M., Elkhateeb S.O., Ali A. and Kharbish S.; 2020a: *Enhancing linear features in aeromagnetic data using directional horizontal gradient at Wadi Haimur area, south Eastern Desert, Egypt*. Carpathian J. Earth Environ. Sci., 15, 323-326.

Eldosouky A.M., Pham L.T., Mohammed H. and Pradhan B.; 2020b: *A comparative study of THG, AS, TA, Theta, TDX and LTHG techniques for improving source boundaries detection of magnetic data using synthetic models: a case study from G. Um Monqul, north Eastern Desert, Egypt*. J. Afr. Earth Sci., 170, 103940.

Eldosouky A.M., Sehsah H., Elkhateeb S.O. and Pour A.B.; 2020c: *Integrating aeromagnetic data and Landsat-8 imagery for detection of post-accretionary shear zones controlling hydrothermal alterations: the Allaqi-Heiani Suture zone, south Eastern Desert, Egypt*. Adv. Space Res., 65, 1008-1024.

Fedi M. and Florio G.; 2001: *Detection of potential fields source boundaries by enhanced horizontal derivative method*. Geophys. Prospect., 49, 40-58.

Ferreira F.J.F., de Souza J., de B. e S. Bongiolo A. and de Castro L.G.; 2013: *Enhancement of the total horizontal gradient of magnetic anomalies using the tilt angle*. Geophys., 78, J33-J41, doi: 10.1190/geo2011-0441.1.

Findlay R.H. and Phan T.T.; 1997: *The structural setting of Song Ma region, Vietnam and the Indochina - South China Plate boundary problem*. Gondwana Res., 1, 11-33.

Foks N.L. and Li Y.; 2016: *Automatic boundary extraction from magnetic field data using triangular meshes*. Geophys., 81, J47-J60.

Hsu S.K., Coppense D. and Shyu C.T.; 1996: *High-resolution detection of geologic boundaries from potential field anomalies: an enhanced analytic signal technique*. Geophys., 61, 1947-1957.

Kafadar O.; 2017: *CURVGRAV-GUI: a graphical user interface to interpret gravity data using curvature technique.* Earth Sci. Inf., 10, 525-537.

Khuong H.T.; 2010: *The complex tectonic events and their influence on formation of mineral deposits in northwest Vietnam*. Ph.D. Thesis in Geology, Geophysics and Environmental Protection, AGH University of Science and Technology, Krakow, Poland, 167 pp.

Lin T.H., Lo C.H., Chung S.L., Wang P.L., Yeh M.W., Lee T.Y., Lan C.Y., Vuong N.V. and Anh T.T.; 2009: *Jurassic dextral movement along the Dien Bien Phu Fault, NW Vietnam: constraints from $^{40}Ar/^{39}Ar$ geochronology*. J. Geol., 117, 192-199.

Liu J., Tran M.D., Tang Y., Nguyen Q.L., Tran T.H., Wu W., Chen J., Zhang Z. and Zhao Z.; 2012: *Permo-Triassic granitoids in the northern part of the Truong Son Belt, NW Vietnam: geochronology, geochemistry and tectonic implications*. Gondwana Res., 22, 628-644.

Ma G., Liu C. and Li L.; 2014: *Balanced horizontal derivative of potential field data to recognize the edges and estimate location parameters of the source*. J. Appl. Geophys., 108, 12-18.

Miller H.G. and Singh V.; 1994: *Potential field tilt a new concept for location of potential field sources*. J. Appl. Geophys., 32, 213-217.

Minh L.H., Hung L.V. and Trieu C.D.; 2001: *Some modern methods of the interpretation aeromagnetic data applied for Tuan Giao region*. Vietnam J. Earth Sci., 22, 207-216.

Nasuti Y. and Nasuti A.; 2018: *NTilt as an improved enhanced tilt derivative filter for edge detection of potential field anomalies*. Geophys. J. Int., 214, 36-45.

Nguyen T.H., Phung P.V., Shakirov R.B., Cao T.D., Phung H.N. and Le A.D.; 2018: *Geoblocks recognition and delineation of the earthquake Prone areas in the Tuan Giao area (northwest Vietnam).* Geotectonics, 52, 359-381.

Oksum E., Dolmaz M.N. and Pham L.T.; 2019: *Inverting gravity anomalies over the Burdur sedimentary basin, SW Turkey*. Acta Geod. Geophys., 54, 445-460.

Oruç B., Sertçelik I., Kafadar O. and Selim H.H.; 2013: *Structural interpretation of the Erzurum Basin, eastern Turkey, using curvature gravity gradient tensor and gravity inversion of basement relief*. J. Appl. Geophys., 88, 105-113.

Pham L.T.; 2020: *A comparative study on different filters for enhancing potential field source boundaries: synthetic examples and a case study from the Song Hong Trough (Vietnam).* Arabian J. Geosci., 13, 723.

Pham L.T., Le-Huy M., Oksum E. and Do T.D.; 2018a: *Determination of maximum tilt angle from analytic signal amplitude of magnetic data by the curvature-based method*. Vietnam J. Earth Sci., 40, 354-366.

Pham L.T., Oksum E., Do T.D. and Le-Huy M.; 2018b: *New method for edges detection of magnetic sources using logistic function*. Geofizicheskiy Zhurnal, 40, 127-135.

Pham L.T., Oksum E., Do T.D., Le-Huy M., Vu M.D. and Nguyen V.D.; 2019: *LAS: a combination of the analytic signal amplitude and the generalised logistic function as a novel edge enhancement of magnetic data*. Contrib. Geophys. Geod., 49, 425-440.

Pham L.T., Oksum E., Do T.D. and Vu M.D.; 2020: *Comparison of different approaches of computing the tilt angle of the total horizontal gradient and tilt angle of the analytic signal amplitude for detecting source edges*. Bull. Mineral Res. Explor., 163, 17 pp., doi: 10.19111/bulletinofmre.746858.

Roest W.R., Verhoef J. and Pilkington M.; 1992: *Magnetic interpretation using the 3-D analytic signal*. Geophys., 57, 116-125.

Sertcelik I. and Kafadar O.; 2012: *Application of edge detection to potential field data using eigenvalue analysis of structure tensor*. J. Appl. Geophys., 84, 86-94.

Verduzco B., Fairhead J.D., Green C.M. and MacKenzie C.; 2004: *New insights into magnetic derivatives for structural mapping*. The Leading Edge, 23, 116-119.

Wijns C., Perez C. and Kowalczyk P.; 2005: *Theta map: edge detection in magnetic data*. Geophys., 70, 39-43.

Yuan Y. and Yu Q.; 2014: *Edge detection in potential-field gradient tensor data by use of improved horizontal analytical signal methods*. Pure Appl. Geophys., 172, 461-472.

Zhou M.F., Chen W.T., Wang C.Y., Prevec S.A., Liu P.P. and Howarth G.H.; 2013: *Two stages of immiscible liquid separation in the formation of Panzhihua-type Fe-Ti-V oxide deposits, SW China*. Geosci. Front., 4, 481-502.

Zuo B., Hu X., Liang Y. and Han Q.; 2014: *Detection of gravity field source boundaries using deconvolution method*. Geophys. J. Int., 199, 1527-1543.

Corresponding author: Luan Thanh Pham
Department of Geophysics, Faculty of Physics, University of Science, Vietnam National University
334 Nguyen Trai street, Thanh Xuan, Hanoi, Vietnam
Phone: +84943396406; e-mail: luanpt@hus.edu.vn